Journal of Quantitative Spectroscopy & Radiative Transfer 112 (2011) 361–375

Contents lists available at ScienceDirect

Journal of Quantitative Spectroscopy & Radiative Transfer

journal homepage: www.elsevier.com/locate/jqsrt

Radiative effect differences between multi-layered and single-layer clouds derived from CERES, CALIPSO, and CloudSat data

Jiming Li [a], Yuhong Yi [b,*], Patrick Minnis [c], Jianping Huang [a], Hongru Yan [a], Yuejie Ma [a], Wencai Wang [a], J. Kirk Ayers [b]

[a] Key Laboratory for Semi-Arid Climate Change of the Ministry of Education, College of Atmospheric Sciences, Lanzhou University, Lanzhou 730000, PR China
[b] Science Systems and Applications Inc., Hampton, VA 23666, USA
[c] NASA Langley Research Center, Hampton, VA 23681, USA

ARTICLE INFO

Keywords:
Cloud radiative effect
Layer thickness
Layer top (base) height
Multi-layered cloud
Single-layer cloud

ABSTRACT

Clouds alter general circulation through modification of the radiative heating profile within the atmosphere. Their effects are complex and depend on height, vertical structure, and phase. The instantaneous cloud radiative effect (CRE) induced by multi-layered (ML) and single-layer (SL) clouds is estimated by analyzing data collected by the Cloud–Aerosol Lidar and Infrared Pathfinder Satellite Observation (CALIPSO), CloudSat, and Clouds and Earth's Radiation Energy Budget System (CERES) missions from March 2007 through February 2008. The CRE differences between ML and SL clouds at the top of the atmosphere (TOA) and at the surface were also examined. The zonal mean shortwave (SW) CRE differences between the ML and SL clouds at the TOA and surface were positive at most latitudes, peaking at 120 W m^{-2} in the tropics and dropping to -30 W m^{-2} at higher latitudes. This indicated that the ML clouds usually reflected less sunlight at the TOA and transmitted more to the surface than the SL clouds, due to their higher cloud top heights. The zonal mean longwave (LW) CRE differences between ML and SL clouds at the TOA and surface were relatively small, ranging from -30 to 30 W m^{-2}. This showed that the ML clouds only increased the amount of thermal radiation at the TOA relative to the SL clouds in the tropics, decreasing it elsewhere. In other words, ML clouds tended to cool the atmosphere in the tropics and warm it elsewhere when compared to SL clouds. The zonal mean net CRE differences were positive at most latitudes and dominated by the SW CRE differences.

1. Introduction

Clouds significantly impact global circulation patterns through their interaction with solar and terrestrial radiation [1]. Cloud systems are often inhomogeneous in their horizontal and vertical structure, commonly occurring with multiple layers over a given location [2,3]. Inferences from global radiosonde water vapor profile data indicate that 40% of all cloud systems consist of multi-layered (ML) clouds [4,5]. Many studies have shown that variations in cloud vertical structures affect the atmospheric circulation by altering the vertical gradients of radiative heating/cooling and latent heating [6–9]. Cloud properties, especially their vertical morphology and impact on the radiation budget, still constitute a major uncertainty in general circulation models (GCMs) and in satellite datasets used for studying climate change.

Most studies of ML cloud radiative effects are based on GCMs [10,11], which typically use some simple cloud overlap assumptions, such as random overlap [12] or a mix of random and maximum overlap [13]. These assumptions have different impacts on the computed

* Corresponding author. Tel.: +1 757 951 1698.
E-mail address: yuhong.yi-1@nasa.gov (Y. Yi).

0022-4073/$ - see front matter © 2010 Elsevier Ltd. All rights reserved.
doi:10.1016/j.jqsrt.2010.10.006

climate statistics, and could be the source of significant errors [14,15]. Studies have shown that the response to variations in cloud overlap can include significant changes in radiative heating rates, atmospheric temperature, hydrological processes, and daily variability [14,16]. Surface fluxes are also quite sensitive to the type of cloud overlap [16]. Knowledge of the true vertical distribution of clouds is critical for accurately modeling the climate.

Empirical studies of the effects of cloud vertical structure (CVS) on the global radiation budget are rare. Although the top-of-atmosphere (TOA) radiation budget can be determined fairly accurately from satellite observations, radiative fluxes at the surface and within the atmosphere are generally retrieved by simply assuming that all clouds are single-layered (SL). Neglecting the effects of ML clouds will introduce significant errors in those retrievals. Furthermore, retrievals of cloud properties, such as cloud height, optical depth, phase and particle size [17], used in flux estimates can be compromised because they are typically based on the SL cloud assumption. Inclusion of overlapped clouds in retrievals of radiative flux profiles requires explicit characterization of the cloud property vertical distributions.

The CVS is difficult to measure using passive satellite sensors. Although a variety of techniques have been developed and applied to limited datasets [18–24], none can adequately characterize cloud layering over all surfaces for all cloud combinations. Ground-based radars and lidars have been providing the CVS over surface sites for more than a decade, but they are sparsely distributed, and non-existent over the oceans. In 2006, the Cloud–Aerosol Lidar and Infrared Pathfinder Satellite Observation (CALIPSO) [25] and CloudSat [26] satellites were launched into the same orbit with Aqua and other satellites to form the A-Train constellation. Combined with the MODerate-resolution Imaging Spectroradiometer (MODIS) [27] and the Clouds and the Earth's Radiant Energy System (CERES) [28] scanners onboard Aqua, it is now possible to observationally explore the impact of CVS on the radiation budget. L'Ecuyer et al. [29] have exploited these combined data to derive high-resolution radiative flux profiles and demonstrate their value for examining the sensitivity of the radiation budget to CVS.

The objective of this paper is to quantify the radiative effect differences between ML and SL cloud systems using observational data and to determine whether the occurrence of ML clouds has any significant consequences beyond what can be represented with SL cloud. By not relying on a cloud overlap assumption, this approach will provide an observational basis for evaluating model results that are based on different cloud overlap assumptions. This study should lead to a better understanding of the interactions between cloud overlap and radiation, and provide an empirical basis for properly evaluating the surface radiation flux in climate models.

The data used are described in Section 2. Section 3 presents the distributions of ML and SL cloud fraction and quantifies the radiation effects and differences between ML and SL clouds. Finally, a simple analysis of the differences is provided.

2. Data and methodology

All data used in this study were taken from daytime A-Train measurements. Thus, the derived quantities are valid for only a single local time, ~1330 LT, except over polar regions.

2.1. Satellite data

The CERES instrument measures broadband radiances at the TOA in three spectral regions (shortwave: 0.2–5.0 μm; window: 8–14 μm; longwave: 5–100 μm) with a nadir spatial resolution of about 20 km. These radiances are converted to TOA fluxes using angular distribution models selected according to the scene classification [30,31]. This study employs CERES Single-Scanner Footprint (SSF) data, which are generated by the Fast Longwave and Shortwave Flux (FLASHFlux) project [32], and combine preliminary CERES radiation measurements, MODIS cloud microphysical retrievals [33,34], and ancillary meteorology fields to form a comprehensive, high-quality compilation of satellite-derived cloud, aerosol, and radiation budget data primarily for providing short-term estimates of surface radiation data. The FLASHFlux SSF data are mostly the same as the CERES SSF data; they differ mainly in the calibrations of the broadband fluxes. Because this study focuses on relative differences in the fluxes, the use of the preliminary CERES calibrations should have little influence on the results. Of the more than 160 parameters in the SSF dataset, only a few are used here: geo-location, upwards SW and LW TOA flux, net SW and LW surface flux-Model B [35–37], and clear/layer/overlap percent coverage. The clear/layer/overlap parameter in the CERES datasets has n rows and 4 columns. The first column indicates the amount of clear sky in a CERES footprint; the second and third ones are the lower layer and upper layer cloud coverage in the footprint, respectively. The last column is the amount that the upper cloud overlaps the lower cloud. In this paper, the first column is used to verify that the selected CERES footprints meet the limitation of overcast or clear. Radiation measurements from FLASHFlux SSF were used to estimate the instantaneous cloud radiative effect (CRE), which is defined below. For simplicity, the FLASHFlux SSF data, hereafter, are referred to as CERES data.

The CloudSat 2B-GEOPROF-LIDAR dataset [38], which combines both the CloudSat and CALIPSO data streams to produce the most accurate quantitative description of the location of hydrometeor layers in the atmosphere, was used to retrieve cloud layers. The advantages of this dataset are that (1) the radar signal will penetrate optically thick layers that attenuate the lidar signal; (2) the radar may observe layers of cloud-free precipitation that may not be observed by the lidar; and (3) the lidar will sense tenuous hydrometeor layers that are below the detection threshold of the radar and the tops of optically thin ice cloud layers undetected by the radar. The 2B-GEOGROF-LIDAR dataset consists of cloud layer numbers and the base and top heights of up to five distinct hydrometeor layers in each column of radar footprint.

The spatial resolution of each collocated CALIPSO/CloudSat Pixel (CCP) is about 1.4 km, far smaller than horizontal scale of common cloud systems, so we may assume that the CCP is fully filled by hydrometeors and cloud is homogeneous in the horizontal direction if the CCP is not clear at all. As a result, we can define any CCP as clear (0 layer), SL cloud (1 layer) or ML cloud (≥ 2 layers) based on the number of cloud layers given in the data. The minimum distance between distinct cloud layers is larger than 240 m (vertical resolution of CloudSat).

It is worth mentioning that the most common misclassification in the CloudSat 2B-GEOPROF-LIDAR data set is that dense aerosol layers are sometimes labeled as cloud. In other words, some CCPs that include dense aerosol layers constitute a source of uncertainty in the current analysis. However, inspection of the cloud–aerosol mask has shown that layers are correctly identified as cloud or aerosol about 90% of the time [39]. Thus, the algorithm producing the CloudSat 2B-GEOPROF-LIDAR dataset is still quite good at correctly identifying clouds.

2.2. Data matching

To estimate the CRE for ML and SL clouds, each CERES footprint is collocated with the appropriate CCPs. Fig. 1 shows a schematic diagram of the four-collocation steps. First, the circular area (10-km radius) surrounding the center of each CERES footprint was searched to find all the CCPs. Normally, about 10–20 CCPs were found in each CERES footprint. CERES footprints having fewer than 10 CCPs were not used in this study. Second, the percentages of clear and SL and ML cloud CCPs were calculated for each CERES footprint. Then, each CERES footprint was defined as clear, SL (if 90% CCPs are SL), or ML (if 90% CCPs are ML), according to its clear (over 90% clear) or cloudy percentage (over 90% cloudy). The CERES footprints with the mixed clear, SL and ML CCPs are not considered in this study. Lastly, the parameter "clear/layer/overlap percent coverage" from the CERES SSF data was checked for each CERES footprint. If a CERES footprint was classified as clear at step three, and the SSF parameter "clear/layer/overlap percent coverage" was also over 95% clear, it was reclassified as clear. If a CERES footprint was classified as either SL or ML cloudy at step three, and the SSF parameter "clear/layer/overlap percent coverage" was less than 5%, it was classified as an SL or ML overcast footprint. The aim of using this parameter was to ensure that the limitation of overcast or clear CERES footprints was met. Only clear, SL and ML overcast CERES footprints were used to examine the CRE differences between ML and SL clouds. It is worth noting that there were very few CERES full overcast (100% cloudy) or clear sky (100% clear) samples (footprints) that match with the CCP data. That is, some clear sky or SL (ML) clouds maybe present in the ML

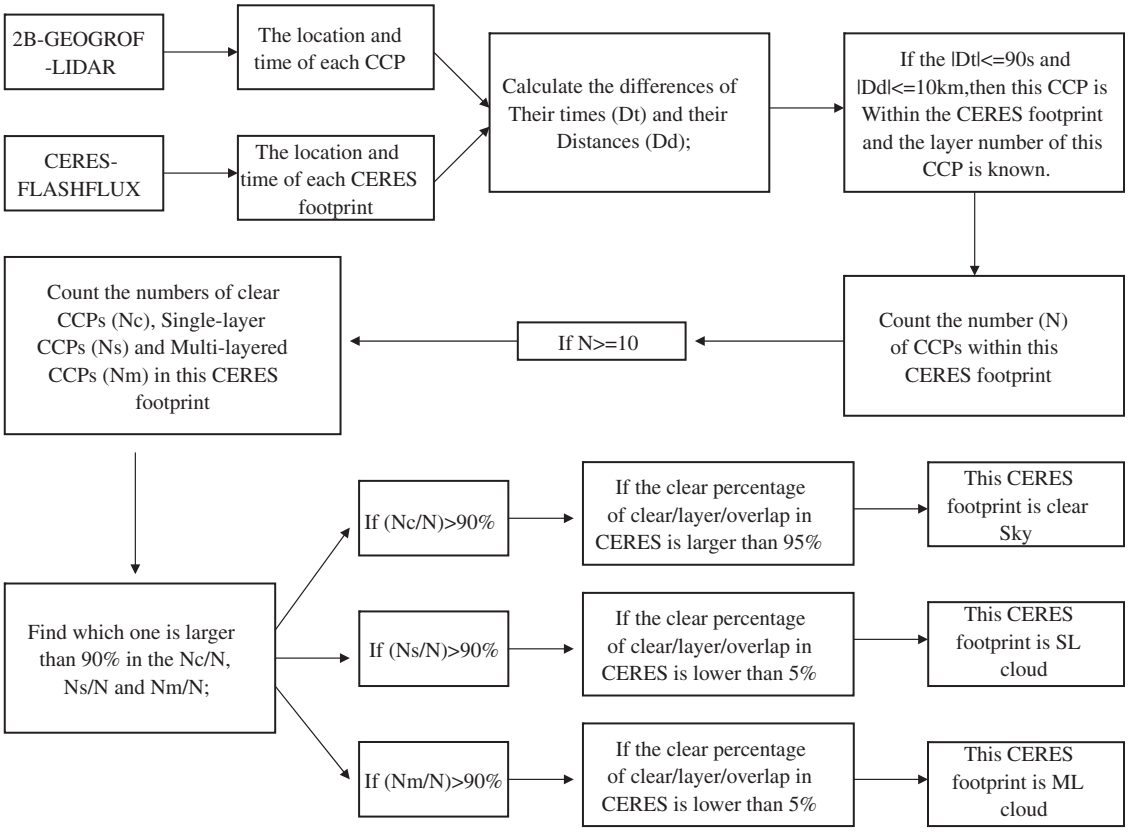

Fig. 1. Schematic diagram of a CERES footprint matched with merged CALIPSO and CloudSat pixels (CCP).

Table 1
Number of CERES footprint in different latitude zones for clear sky, SL, and ML clouds.

	Global (90° N–90° S)	Tropical (20° N–20° S)	Mid-latitude (20–60° N, 20–60° S)	High-latitude (60–90° N, 60–90° S)
Clear sky (clear pct > 90%)	308840	84012	184190	40638
Single-layer (cloudy pct > 90%)	540731	97188	321816	121727
Multi-layer (cloudy pct > 90%)	317384	110439	164254	42691

(SL) cloud samples. Although very few scenes were contaminated with incorrectly identified pixels, those misidentified pixels are a potential source of uncertainty in the results. Table 1 lists the numbers of selected CERES footprints on a global scale and for different latitude regions. The tropics are defined as latitudes between 20° S and 20° N, mid-latitudes as 20–60° N and 20–60° S, and high latitudes were from 60° to 90° S and 60° to 90° N. About 60% of the clear or SL CERES footprints were found in the mid-latitudes, with 35% and 51% of the ML CERES footprints found in the tropical and mid-latitudes, respectively. In this study, we found that about 38% of ML cloud samples selected by using the collocation steps (see Fig. 1) were considered as SL clouds by MODIS. At least part of the ML cloud dataset like this may consist of one optically thin cloud layer overlapping a thicker water cloud. In other words, the retrieval of cloud optical properties in the CERES SSF data may be affected by the existence of ML clouds. Since the radiation flux parameters of CERES SSF data were used in this study, the CRE results at surface will be affected by ML clouds. In addition, all selected samples are from instantaneous observations, the annual mean cloud properties (e.g., cloud fraction, CRE and so on) were obtained by simply averaging all samples during the 1-year study period.

2.3. Cloud radiative effect (CRE)

The CRE, sometimes referred to as cloud radiative forcing, is a very important parameter that has been used to quantify the degree of cloud–radiation interactions. It is defined as the radiative impact that clouds have on the atmosphere, surface, or TOA relative to a clear sky [40,41]. One aim of this study is to evaluate the impact of clouds on TOA and surface fluxes. Therefore, the CERES outgoing SW and LW TOA fluxes and Model-B net SW and LW surface fluxes were used in the study.

In general, the SW and LW cloud effect parameters are defined as

$$CE_{SW} = (F_{SW}^{down}\text{-}F_{SW}^{up})^{cloudy}\text{-}(F_{SW}^{down}\text{-}F_{SW}^{up})^{clear},$$
$$CE_{LW} = (F_{LW}^{down}\text{-}F_{LW}^{up})^{cloudy}\text{-}(F_{LW}^{down}\text{-}F_{LW}^{up})^{clear},$$
$$CE_{NET} = CE_{SW} + CE_{LW} \quad (1)$$

where F_{SW}^{down} (F_{SW}^{up}) and F_{LW}^{down} (F_{LW}^{up}) are the downward (upward) SW and LW fluxes, respectively. "Cloudy" and "clear" indicate overcast and clear-sky conditions, respectively.

At the TOA,

$$(F_{SW}^{down})^{cloudy} = (F_{SW}^{down})^{clear},\ (F_{LW}^{down})^{cloudy} = (F_{LW}^{down})^{clear} = 0$$

Thus, Eq. (1) changes to

$$CE_{SW} = (F_{SW}^{up})^{clear} - (F_{SW}^{up})^{cloudy},$$
$$CE_{LW} = (F_{LW}^{up})^{clear} - (F_{LW}^{up})^{cloudy} \quad (2)$$

The SL and ML CRE at the TOA were calculated with Eq. (2) using the upward SW and LW TOA fluxes in the CERES dataset.

At the surface,

$$CE_{SW} = (F_{SW}^{net})^{cloudy}\text{-}(F_{SW}^{net})^{clear},$$
$$CE_{LW} = (F_{LW}^{net})^{cloudy}\text{-}(F_{LW}^{net})^{clear} \quad (3)$$

Therefore the CRE from Eq. (3) could be calculated using the net SW and LW surface fluxes (Model B) in the CERES dataset.

3. Results

3.1. Global and zonal distributions of ML and SL clouds

Cloud fraction and type are two critical factors in cloud–radiation feedback. Many previous studies of cloud radiative effects have focused on the relationship between the Earth radiation budget at the TOA and the cloud cover [42,43]. When the cloud fraction increases, more sunlight will be reflected to space, which will change cloud radiative effects. Only overcast CERES footprints were used here, so the effect of fractional cloud cover on the radiation flux will not be discussed. However, it is still essential to know the global and zonal distributions of cloud fraction for ML and SL clouds before analyzing the ML and SL CRE.

Multi-layered clouds, namely overlapping cloud layers, commonly occur in the vicinity of fronts and around deep tropical convection [12]. In this study, we calculated the cloud fraction and cloud amount by using the merged CALIPSO/CLOUDSAT observations during March 2007 through February 2008. It is worth noting that cloud fraction and cloud amount have different meanings in this study. Cloud fraction for a given grid box is defined as the number of total cloud, SL or ML cloud profiles divided by the total number of sample profiles collected in a given grid box. The cloud amount in a given grid box is defined as the number of SL or ML cloud profiles divided by the number of total cloud profiles collected in a given grid box. Similar definitions for cloud fraction were also used by Hagihara et al. [44].

Fig. 2 shows the global distribution of total, SL, and ML cloud fractions. Total cloud fraction is relatively low over northern and southern Africa, the Middle East, northern China, Australia, southern South America, and Antarctica. The cloud fraction is less than 30% over parts of the Sahara

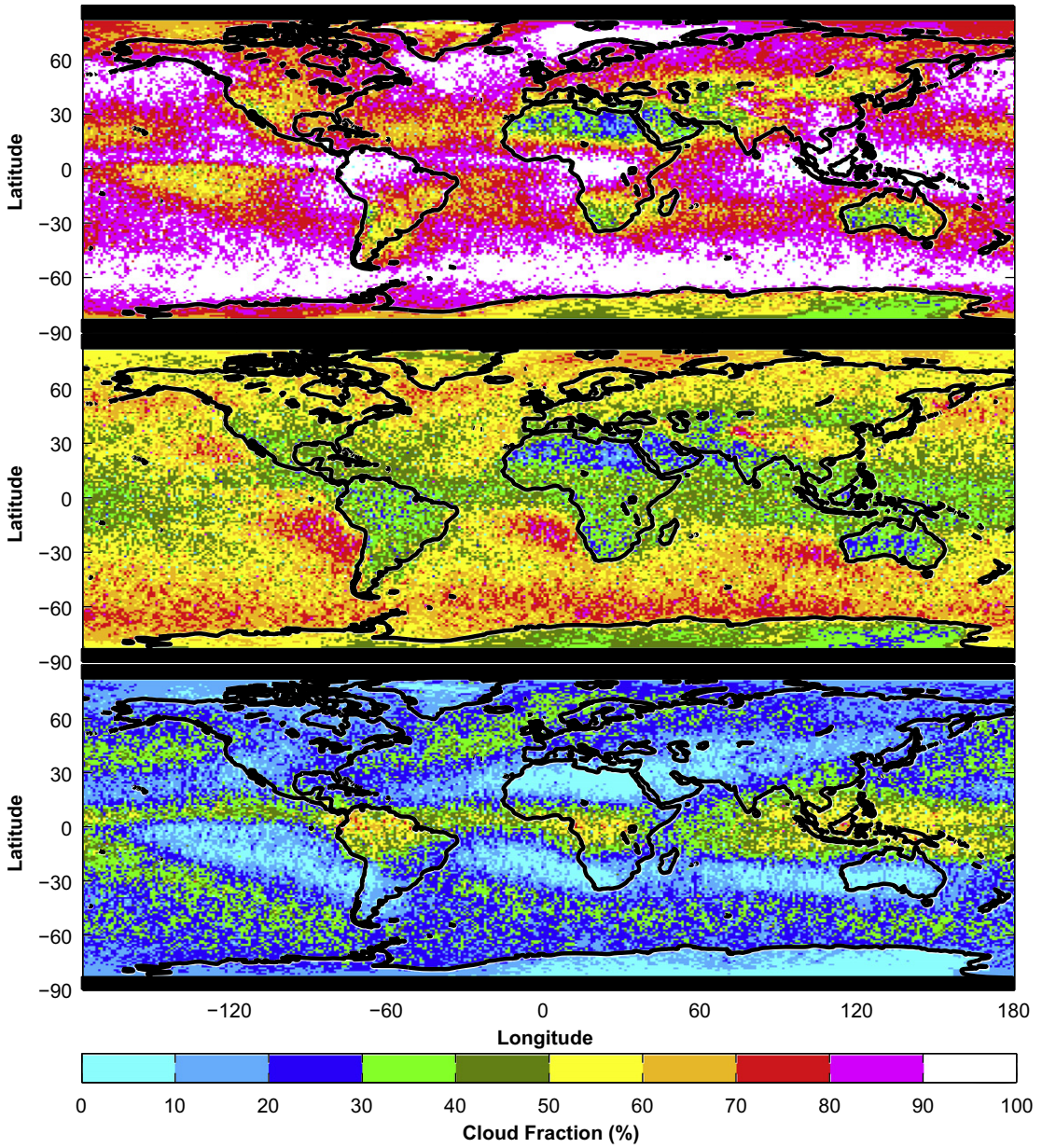

Fig. 2. Global distributions of the total, SL, and ML cloud fractions (%) from March 2007 to February 2008. Top, middle, and bottom panels show the total, SL, and ML cloud fractions, respectively.

Desert. Conversely, the cloud fraction is large (greater than 80%) over the ocean at mid- and high-latitudes in the Southern Hemisphere (SH) and over northern South America, central Africa, and the high latitudes of the Northern Hemisphere (NH). Except for a few areas in the tropics, the fraction of SL cloud cover exceeds the ML cloud fraction for the whole year over the globe. The SL cloud fraction is generally small wherever the total cloud cover is minimal. Greater values are seen over the ocean at mid- and high-latitudes in the SH, and on the western coasts of land at low latitudes. The ML cloud fraction is greatest over northern South America, central Africa, the ocean near Indonesia, and the oceans in the NH. Meanwhile, the lowest values of ML cloud fraction are found over land in the NH, Australia and over ocean at low latitudes in the SH. There is little ML cloud cover over Antarctica. On the whole, the cloud fraction is larger over oceans than over land. Overall, the global mean total cloud fraction is about 77.4%, while the SL and ML cloud fractions are 51.6% and 25.8%, respectively. The global mean SL and ML cloud amounts are 67.7% and 32.3%, respectively. The total cloud fraction results were very similar to those reported by Mace et al. [38] for a different, but overlapping time period. Winker et al. [45] showed that global average cloud cover measured by the CALIPSO is about 75%, significantly higher than existing cloud

climatologies due to sensitivity of CALIOP to optically thin clouds. Wylie and Jackson [46] also obtained similar results by using two decades of HIRS observations, and indicated that total cloud cover remains relatively steady over the 22 years studied, with roughly 75% of all HIRS observations indicating clouds.

Fig. 3 shows the zonal distributions of ML and SL cloud fractions and cloud amounts from March 2007 through February 2008. As described above, cloud amount is defined as the fraction of ML or SL cloudiness to the total cloud fraction. Thus, it measures the percentage of the observed clouds that were either SL or ML clouds. The zonal total and ML cloud fractions are clearly largest in three regions: the equatorial zone and the mid-latitudes in both hemispheres (near 60°). This pattern corresponds to the ascending flows of the Hadley and Ferrell circulations. The total cloud fraction maximum in the tropical zone is 90% at 6° N, the only zone where the ML cloud fraction exceeds its SL complement. Near 60° S, the largest total cloud fraction is 95% and is primarily due to SL cloud systems. Near 60° N, the largest total cloud fraction is 85%, the smallest of the three zones. The minima in total cloud fraction are found over Antarctica and near 22° S and 22° N. The ML cloud fraction distribution follows the total cloud distribution, except that the mid-latitude maxima are much reduced relative to the tropical peak. The SL cloud fraction distribution is different. It increases with latitude from its equatorial minimum, decreasing only at 60° S. On average, the SL cloud amount is larger than the ML cloud fraction by 35%. It accounts for ~75% of all clouds south of 25° S and 70% north of 25° N. The largest ML cloud amount (smallest SL cloud amount) was approximately 53% (47%) in the tropics.

3.2. Zonal distributions of SL and ML cloud top height and layer thickness

It is well known that clouds both reflect solar SW radiation to space and reduce the emission of LW radiation. However, clouds at different levels have different radiative effects, due to differences in temperature and optical depth. Generally speaking, high-level clouds (such as cirrus) enhance atmospheric warming. They are highly transparent to solar SW radiation but readily decrease outgoing LW radiation because of their lower temperatures. Conversely, low clouds have a cooling effect, as they reflect more solar energy to space and have a relatively small impact on the outgoing LW radiation. This is because they are near the surface and at almost the same temperature as the surface. The effect of mid-level clouds depends on the relative strength of these two effects. The CRE of low, high, and mid-level clouds has been discussed in a number of studies [47].

The factors that influence CREs are numerous and complicated. In general, the LW CRE is primarily determined by cloud temperature, height, and emissivity. The SW CRE is determined by the solar zenith angle, surface albedo, and cloud transmittance and albedo. However, due to the difficulty of acquiring these microphysical properties for multilayer clouds, only the relationship between the CRE and cloud macro-physical properties (cloud top, base height and cloud thickness) are analyzed in this paper.

Unlike the cloud fraction, the cloud properties were derived from all selected CERES footprints. All samples were first averaged onto a $1^\circ \times 1^\circ$ grid, and then used to calculate zonal averages. The zonal distributions of cloud top height (CTH), cloud base height (CBH), and cloud layer thickness (CLT) during March 2007 through February 2008 are shown in Fig. 4. Clearly, the ML CTH (uppermost layer) is always higher than the SL CTH. Both the ML and SL CTH have tropical maxima, with values of 13 and 15 km for SL and ML clouds, respectively. The two maximum values of the CTH difference are 8.5 and 7 km at 20° in the SH and NH, respectively. The minimum value is 2 km in the NH tropics.

The CBH of the SL clouds is generally higher than that for ML clouds. Fig. 4 shows that the ML CBH

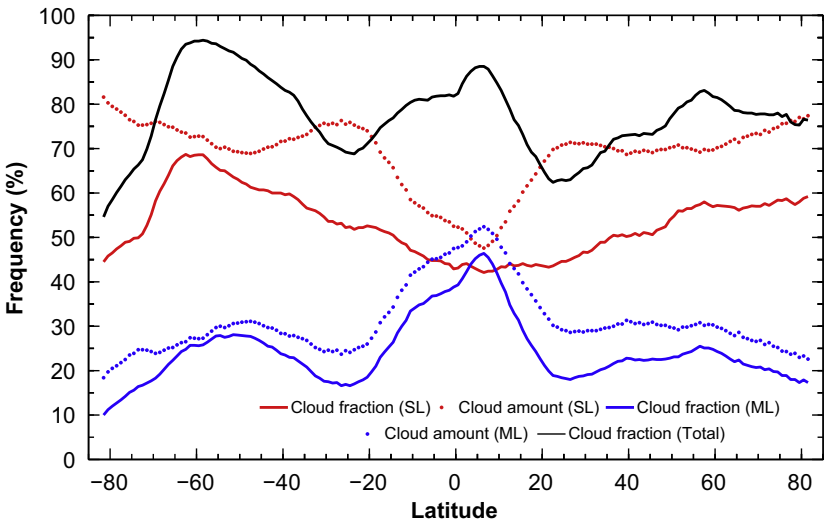

Fig. 3. Zonal distributions of the cloud fraction (solid lines) and relative cloud amount (dotted lines) for total, SL, and ML clouds during the full-year period from March 2007 to February 2008.

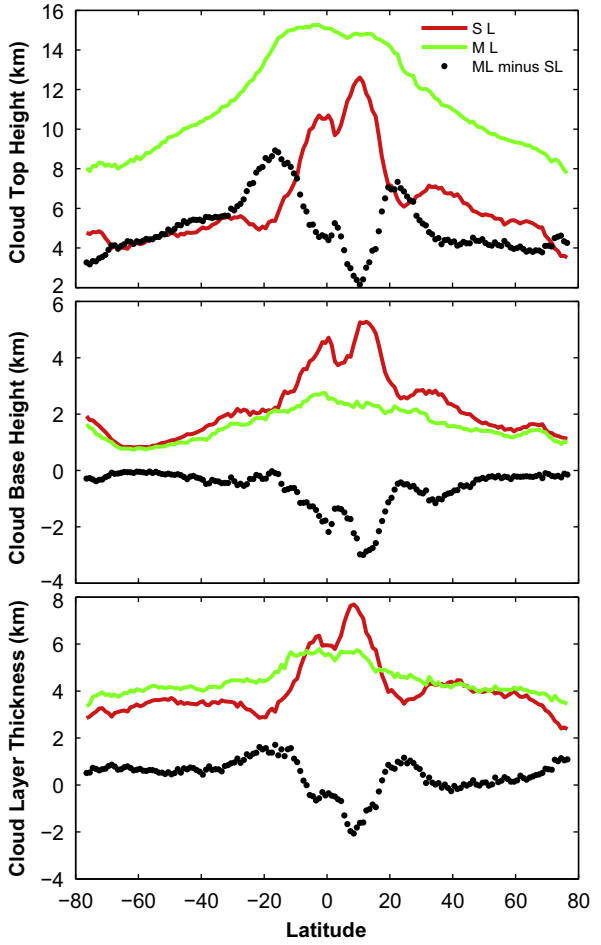

Fig. 4. Zonal distributions of cloud top height (top panel), cloud base height (middle panel), and cloud layer thickness (bottom panel) for SL and ML clouds during the full-year period from March 2007 through February 2008. The dotted lines are the differences between ML and SL clouds. For ML clouds, the cloud top height, cloud base height, and layer thickness are for the uppermost cloud layer, the lowermost cloud layer, and the sum of all cloud layer thicknesses, respectively.

(lowermost layer) is about 2.5 km, at most, in the tropics. However, the mean SL cloud base height is as high as 5.5 km in the tropics, so their maximum difference is about 3 km. The maximum SL and ML cloud thicknesses of 7.5 and 5.5 km, respectively, also occurred in the tropics. The SL cloud thickness exceeds its ML counterpart in the NH tropics, by up to 2 km. The difference is less than 2 km elsewhere.

3.3. Distributions of the SL and ML CRE differences

Fig. 5 shows the global distributions of the SW, LW, and net CRE differences between ML and SL clouds at the TOA and the surface. The SW CRE difference is positive at the TOA and surface in the tropics, with values greater than 120 W m^{-2} north of South America and in the ocean around Indonesia. The SW CRE difference at the surface in the tropics and over the oceans in the SH is positive over a larger area than at the TOA. For the LW CRE difference, the TOA and surface distributions are very different. The LW CRE difference has minima of -50 W m^{-2} north of South America, in central Africa, and over the ocean near Indonesia at the TOA. The LW CRE difference has positive maxima of $\sim$50 W m^{-2} on the western coast of South America, southern Africa, and Australia at the TOA. However, the LW CRE difference at the surface is not as obvious as that at the TOA, as it varies from -20 to 20 W m^{-2}. Both the global distribution and magnitude of Net CRE differences are similar to those of the SW CRE differences because the SW CRE difference is quite larger than the LW CRE difference and dominated in Net CRE differences.

Fig. 6 shows the zonal distributions of SL and ML CRE and their differences at the TOA (Fig. 6a-c) and surface (Fig. 6d-f). The red, green, and blue lines represent SL and ML cloud samples and their differences, respectively. As stated in Section 2.2, we found that about 38% of ML cloud samples selected by using the collocation steps (Fig. 1) were considered as the SL cloud by MODIS. To study the CRE from these ML cloud samples (hereafter, to distinguish this part ML cloud (green dotted lines) from all ML cloud samples (green solid lines) in Fig. 6, we denote this ML cloud as "ML1"), and separately compared the CRE of ML1 clouds with SL clouds.

For the SW CRE at the TOA, the SL and ML cloud values both reach a maximum in the tropics, then decrease toward both polar regions. The SW CRE for SL (ML) clouds in the tropics of the NH drops as low as -400 W m^{-2} (-300 W m^{-2}). The SW CRE difference between the ML and SL clouds is positive and largest in the NH tropics, where it reaches 120 W m^{-2}. The differences diminish toward high latitudes. The SW CRE distribution at the surface is similar, with the SL SW CRE falling below -400 W m^{-2}. However, the ML SW CRE at the surface is slightly higher in the mid-latitudes than in the tropics, with some negative differences in the polar regions. The distributions of SW CRE values for ML1 cloud (green dotted line) are similar to those for ML clouds (green solid line), but ML1 clouds have larger SW CRE than ML clouds. The difference in SW CRE between ML1 and SL clouds are relatively smaller (from -50 to 50 W m^{-2}, blue dotted lines), while the opposite difference is present over the tropics in the two hemispheres (Fig. 6a).

The LW CRE for ML and SL clouds at the TOA (Fig. 6b) decreases from the tropics to the poles in both hemispheres. The SL (ML) CRE is 120 W m^{-2} (90 W m^{-2}) at the equator, while at the poles, the LW CRE is only about 25 W m^{-2} for both cloud types. The LW CRE difference between the ML and SL clouds at the TOA is negative only in the northern tropics and around 35° N. The LW CRE differences are most pronounced in the tropics and around $\pm 20°$ latitude, where the values were -30 and 30 W m^{-2}, respectively. The distribution of the LW CRE at the surface (Fig. 6d) is opposite to that at the TOA (low in the tropics and high at high latitudes), with values of 35 and 90 W m^{-2}, respectively. The surface LW CRE difference between ML and SL clouds is very small, between -10 and 10 W m^{-2}. The distributions of LW CRE for ML1 cloud (green dotted line) are also similar to ML (green solid line) but ML1 clouds had larger LW CRE than the ML clouds. The LW CRE difference is positive at most latitudes (Fig. 6b, blue dotted line). Because the SW CRE differences

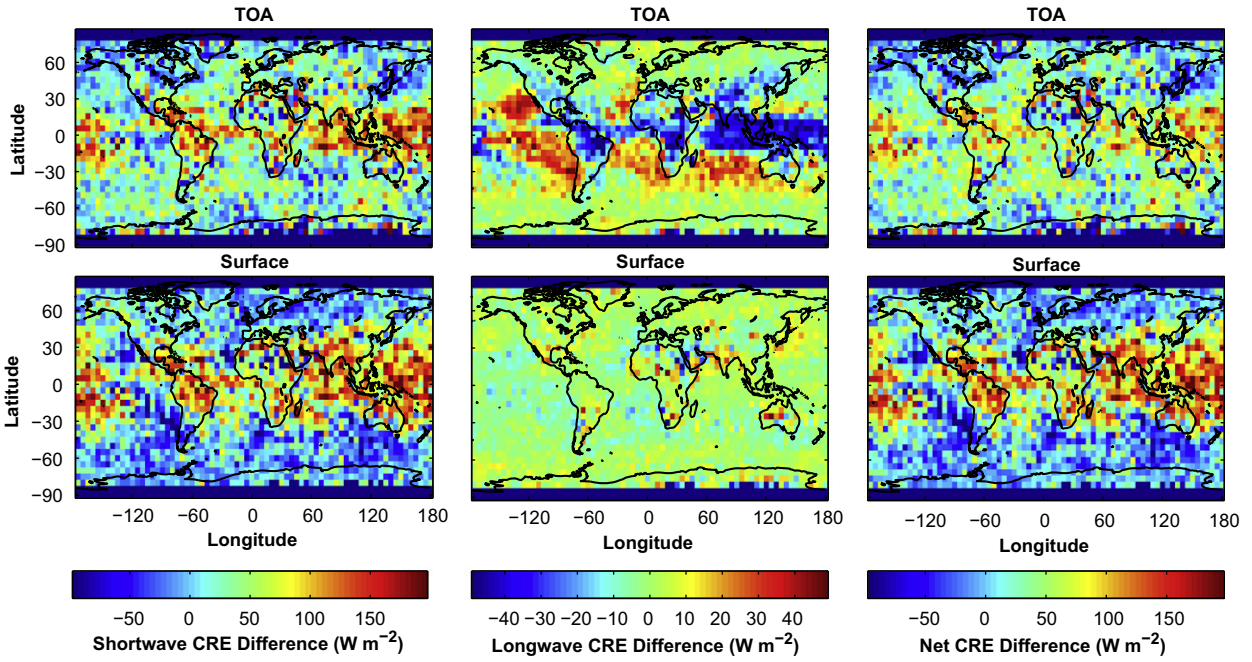

Fig. 5. Mean SW (left), LW (center), and Net (right) CRE differences between ML and SL clouds at the TOA (top panels) and the surface (bottom panels), March 2007–February 2008, ~1330 LT.

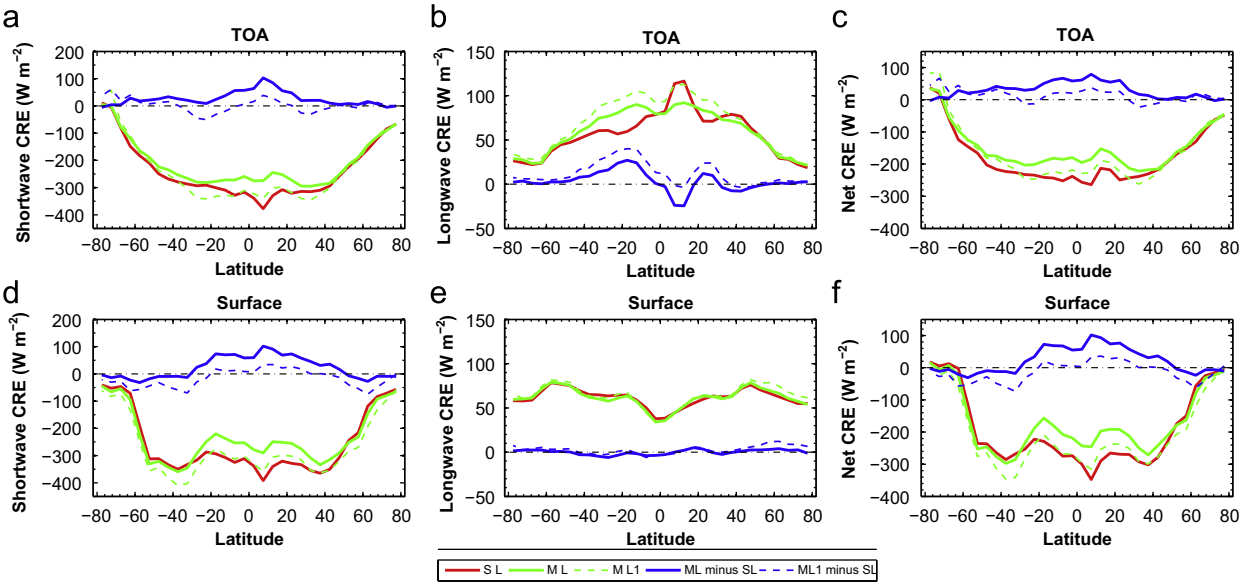

Fig. 6. Zonal distributions of SL and ML CRE and their differences at the TOA (top panels), and the surface (bottom panels), March 2007–February 2008. Left column: SW CRE; middle: LW CRE, and right: Net CRE. SL (red), ML (green), ML-SL (blue). Solid lines denote all ML clouds selected using collocation steps. Dashed lines indicate results using only ML clouds missed by MODIS (ML1).

are much larger than the LW CRE differences, the zonal distributions and magnitudes of the TOA (Fig. 6c) and surface (Fig. 6f) Net CREs and differences are both similar to their SW CRE counterparts.

In summary, ML clouds reflected less sunlight to the TOA, than SL clouds, thus allowing more SW radiation to reach the surface (Fig. 6a and d). In general, ML clouds increased thermal radiation at the TOA compared to SL clouds only in the tropics and decreased it elsewhere, but the differences were always less than ± 30 W m^{-2}. There are negligible differences between the ML and SL LW CRE at the surface. Because the SW CRE difference was far larger than the LW CRE difference, it dominates the zonal distribution and magnitude of the net CRE and difference.

It is a given that some uncertainties or biases were present in CRE results. Two uncertainty sources, aerosols identified as clouds and some clear (cloudy) contamination of the cloudy (clear) samples, were mentioned in the Sections 2.1 and 2.2. The mistaken identity of the aerosols as clouds occurs in less than 10% of the data and should have a minor impact on the results. The contaminated footprint percentages (about 0–10%) of clear sky or SL (ML) cloud that may be present in the ML (SL) cloud samples are relatively small, so that the impact on the CRE results should also be small. Although there are some uncertainties or biases present in this study, the results should be reliable and without substantive variation. The top-of-atmosphere (TOA) radiation budget can be determined fairly accurately from satellite observations and its accuracy is not strongly dependent on cloud vertical distribution. However, surface radiation flux analysis depends on the assumption that all clouds are single-layer, so the SL CRE values at the surface are more reliable than those for the ML CRE. All of the surface results are less reliable than those at the TOA.

3.4. Distributions of SW CRE and LW CRE

Figs. 7 and 8 show density plots of TOA and surface, respectively, SW and LW CRE pairs in terms of the number of samples for different latitude zones during the period, March 2007–February 2008. Four relatively distinct features in Fig. 7 are evident for SL clouds. In the tropics (Fig. 7c) and mid-latitudes (Fig. 7e), there is an ellipsoid of CERES footprints corresponding to relatively small LW CRE values, $< 50\ \mathrm{W\,m^{-2}}$, having SW CRE values between -400 and $-100\ \mathrm{W\,m^{-2}}$. The third feature is an exponential curve beginning near the zero point and asymptoting at LW CRE $\approx 180\ \mathrm{W\,m^{-2}}$, but extending to SW CRE values $< -600\ \mathrm{W\,m^{-2}}$. This third feature is simply a cutoff of that exponential curve. The ellipsoid and curve correspond to SL low and high clouds, respectively. In the tropics, the curve and cluster of points is very distinct suggesting that few mid-level clouds occur alone in the tropics. The two features become fuzzier in the mid-latitudes and disappear in the polar zones (Fig. 7g), where they are replaced by a relatively featureless cloud of points with LW CRE between 0 and $50\ \mathrm{W\,m^{-2}}$ and SW CRE between $-400\ \mathrm{W\,m^{-2}}$ and values exceeding $150\ \mathrm{W\,m^{-2}}$, indicated by the cluster at $150\ \mathrm{W\,m^{-2}}$. The cloud of points is over a line of points at LW CRE $\approx -20\ \mathrm{W\,m^{-2}}$. This linear feature corresponds to low clouds over a warmer surface, such as open water. These four features give rise to the pattern in Fig. 7a.

For ML clouds, the ellipsoids and curves are replaced by more diffuse, almost featureless clusters between the two features seen for SL clouds in the tropics (Fig. 7d) and mid-latitudes (Fig. 7f). The cutoff features are no longer apparent suggesting that the SW CRE minima are mostly

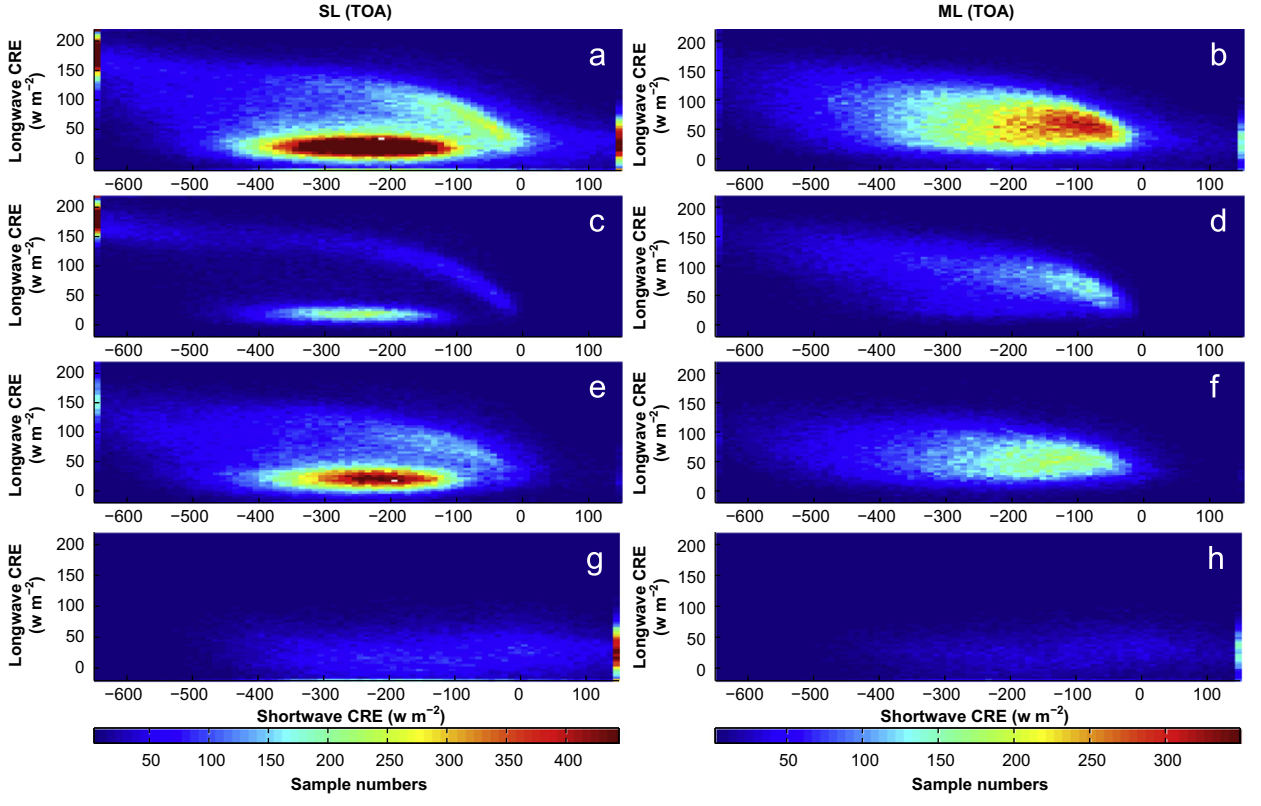

Fig. 7. Density plots of TOA SW and LW CRE pairs in different latitude zones, March 2007–February 2008. (a) and (b) global; (c) and (d) tropics; (e) and (f) mid-latitude; (g) and (h) high latitude. Left panels are for SL clouds, right for ML clouds.

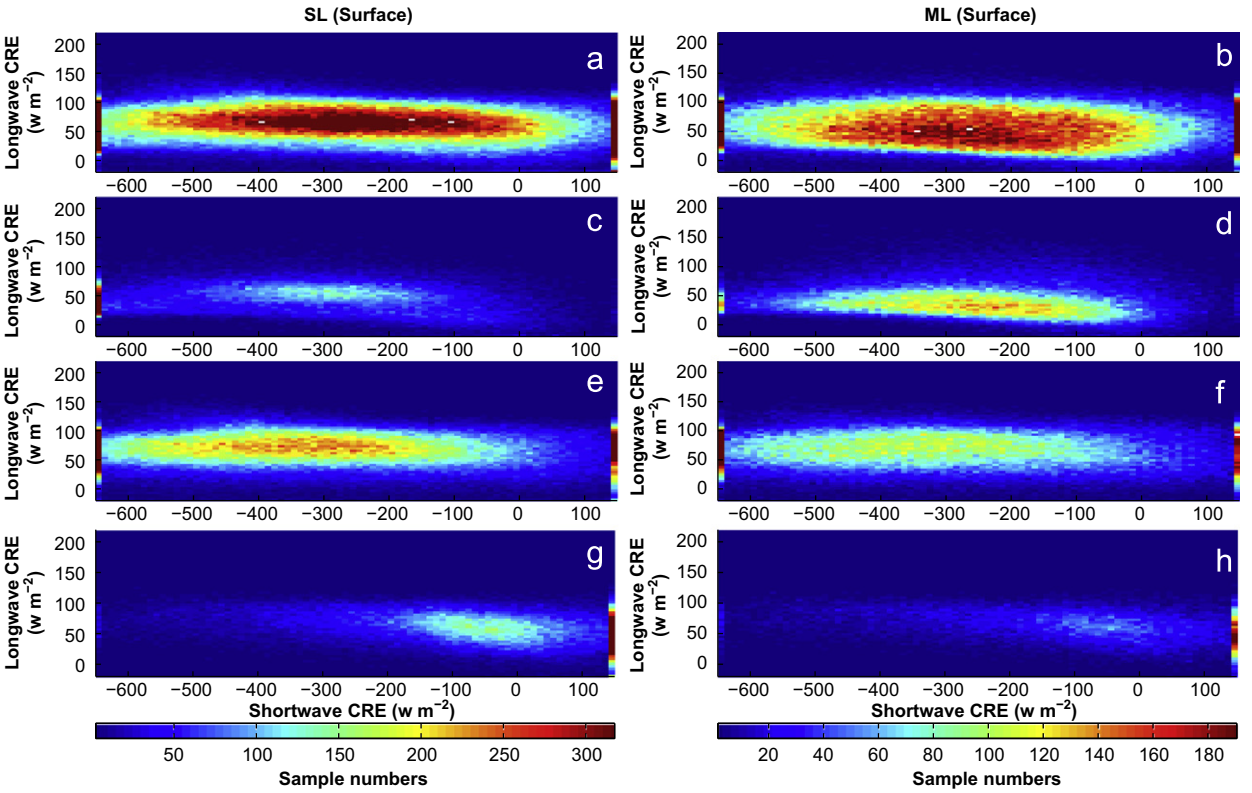

Fig. 8. Same as Fig. 7, except for surface SW and LW CRE pairs.

due to very thick contiguous clouds and not ML systems. In the polar zones (Fig.7h), the cloud of points becomes more nebulous and the linear feature disappears.

For the surface CRE pairs in Fig. 8, the ML and SL cloud samples have similar distributions, although the SL features are more distinct. Globally, the SL clouds (Fig. 8a) have a peak concentration of points at $\sim$70 W m^{-2} compared to the ML peak near 50 W m^{-2} (Fig. 8b). Much like the results in Figs. 8c and d, the ML SW CREs in Fig. 8d are closer to zero than the SL values (Fig. 8c). This effect is not so pronounced for the mid-latitudes (Fig. 8e, f). In the polar regions (Fig. 8g, h), there is no significant difference between the SL and ML CRE pairs except for the greater number of points for the SL clouds. It is worth further noting the clusters on the left and right boundaries of Figs. 7 and 8. Because the CRE results in this study are from instantaneous radiation fluxes, many CERES fluxes exceeded 800 W m^{-2}. Thus, SW CRE < -600 W m^{-2} occurred in many cases. On the right boundaries, SW CRE is strongly positive at the middle- or high-latitudes (many points at +150 W m^{-2}), but the zonal means are nearly all negative (Fig. 6). We found that the positive results mainly occurred for solar zenith angles greater than 78°.

3.5. Relationships among CRE, layer thickness, and layer height

Figs. 9–13 show the variation of mean TOA CRE for the combinations of cloud layer thickness (CLT) and top height (CTH) observed from March 2007 to February 2008 for both SL and ML clouds. For ML clouds, CTH is the cloud top height of the uppermost cloud layer, and the CLT is the sum of thickness of all cloud layers contained in the cloud column. The top and middle panels in each figure plot mean CRE for SL and ML clouds, respectively, for pairs of CLT and CTH. Their differences are given in the bottom panels. Overall, the SL and ML TOA SW CRE (Fig. 9) distributions are similar except for some differences in magnitude. The most obvious feature is that the SW cloud cooling effect (negative SW CRE) is increases with CLT for both SL and ML clouds. When the clouds are high but relatively thin (CTH > 8 km and CLT < 4 km, cirrus and cirrostratus), the cloud cooling effect of the ML clouds is larger than that of the SL clouds. The SW CRE differences between ML and SL clouds are negative when clouds are thinner and higher. In other words, ML clouds reflect more sunlight to TOA than SL clouds indicating that ML clouds enhance SW cloud cooling effects and cool the earth–atmosphere system more than SL clouds. When the clouds are high and deep (CTH > 8 km and CLT > 6 km), the SW cloud cooling effects for the SL and ML clouds are both large (|SW CRE| ranges from 300 to 600 W m^{-2}) but the SL cooling effect tends to be greater than that for ML clouds (ML–SL > 0 W m^{-2}). Such high-topped, thick SL clouds are mostly deep convective clouds, also the brightest clouds. Thick cirrus over thick water clouds could yield similar combinations of CTH and CLT, but would tend to have lower albedos. The occurrence of a few positive (dark blue) SW CRE values is likely due to a combination of a small number of samples having clear-sky

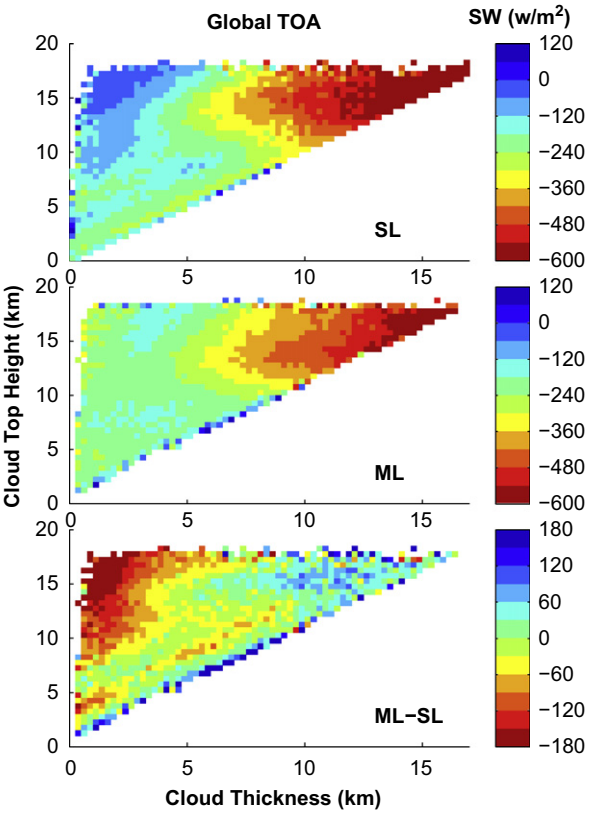

Fig. 9. Global $1^\circ \times 1^\circ$ degree box mean TOA SW CRE as a function of cloud thickness and cloud top height, March 2007–February 2008.

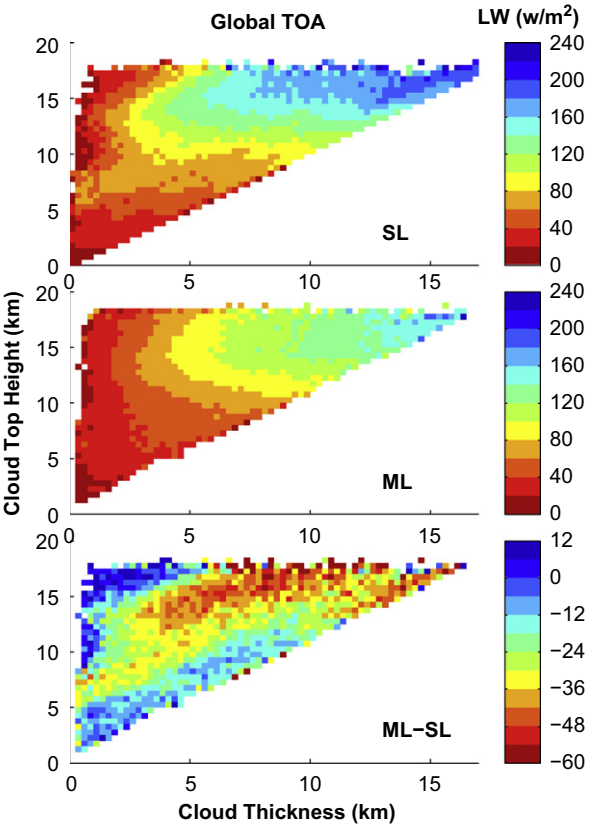

Fig. 10. Same as Fig. 9, except for TOA LW CREs.

flux uncertainties larger than the SW CRE that is being computed.

The LW cloud warming effects (positive LW CRE) generally increase with increasing CTH and CLT for both SL and ML clouds (Fig. 10). Again, the deep, high clouds produce the greatest CRE, and the SL values are greater than their ML counterparts. For thinner clouds, LW CRE does not always increase with cloud top height. The LW CRE differences between ML and SL clouds show 3 different regimes. When the CLT is smaller than 4 km, and the CTH is 13 or 14 km or higher, the LW CRE difference between ML and SL clouds is slightly positive, that is, ML clouds would slightly warm the atmosphere more than SL clouds. Conversely, when the CLT exceeds 4 km, and the CTH is higher than 10 km, the LW CRE differences are negative everywhere. This indicates that the LW cloud warming effect for SL clouds is generally larger than for ML clouds.

Fig. 11 shows the relationships among CTH, CLT, and TOA NET CRE. Since the SW CRE contribution dominates the NET CREs, the distributions of NET CREs are much like those for the SW CREs. Deep convective clouds have large NET CREs (absolute values) ranging from -350 to -550 W m^{-2}. This indicates that the deep convective clouds have a strong cloud cooling effect, but the NET CRE for thinner (<4 km) SL clouds is very small (-100 W m^{-2} to zero). For SL clouds, NET CRE also varies with cloud top height, near -250 W m^{-2} for low clouds to -100 W m^{-2} for high clouds. For ML clouds, the large net cloud cooling effects (large negative NET CRE) occur in areas where clouds are higher and thicker. High, thick ML clouds produce a slightly smaller cooling effect than their SL counterparts as seen by the positive differences. In general, the NET CRE for ML clouds is larger than for SL clouds having similar CTH and CLT when CLT <9 km. That is, the NET CRE difference between ML and SL cloud is negative (-35 to -175 W m^{-2}). The greatest differences appear when CLT <2 km and CTH >8 km. This may be caused by the structure of the ML clouds, that is, a thin cloud layer overlapping a thick low cloud layer, so that the ML cloud has a larger SW CRE, and in turn, large NET CRE.

The NET CRE dependence on CTH and CLT is broken down according to latitude in Fig.12. The features for SL and ML clouds in the tropical and mid-latitude regions are similar to the global features (Fig. 11) but the high-latitude region features are significantly different. Very few positive ML–SL differences and large differences seen only for the thinner clouds in other zones are found for most combinations of CLT and CTH.

Surface Net CREs for SL and ML clouds and their differences are shown as functions of cloud thickness, cloud top height, or cloud base height from March 2007 to February 2008 are shown in Fig. 13. Similar to TOA Net CREs, when clouds are high and thick, the surface net cloud cooling effects are larger for both SL and ML clouds.

When clouds are relatively thin (less than 5 km), the cloud cooling effects are relatively small, as expected. However, the ML clouds exhibit less cloud cooling than SL clouds with similar cloud top height and cloud thickness.

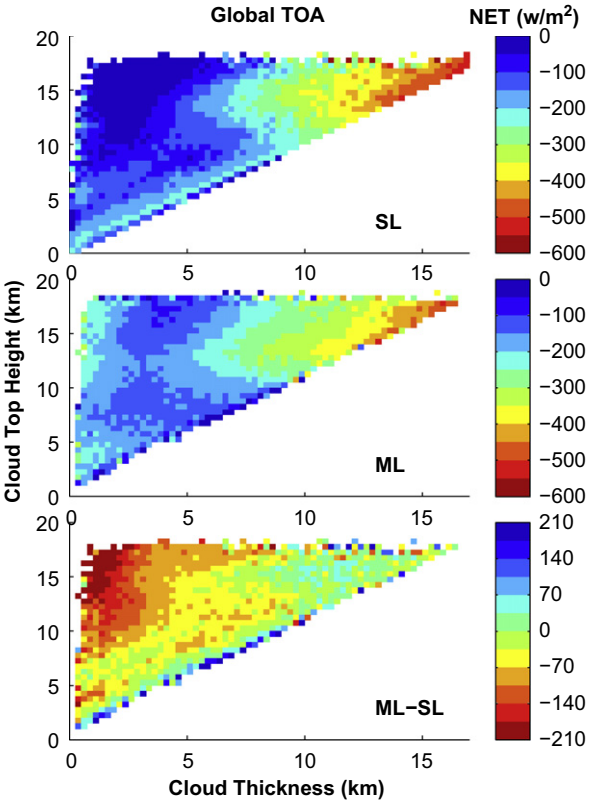

Fig. 11. Same as Fig. 9, except for TOA Net CREs.

4. Summary and discussions

Cloud vertical structure is a crucial factor in climate studies due to its impact on both the magnitude and sign of the CRE and on the heating profile of the atmosphere. However, we have poor knowledge of the extent and frequency of overlapped cloud systems in the atmosphere due to instrument limitations and lack of observations. The importance and impact of CVS on various atmospheric aspects has not really been quantified nor studied thoroughly.

The present study was based on 1 year of CERES SSF data from Aqua and CloudSat 2B-GEOGROF-LIDAR dataset, which combines both CloudSat and CALIPSO data streams, taken from March 2007 through February 2008. The aim of the work was to quantify the radiation effect differences between ML and SL clouds using observational data and to determine whether the occurrence of ML clouds has any significant consequences beyond what can be represented with typical SL cloud assumptions.

The results indicate that ML clouds have a significant impact on CRE due to their high frequency of occurrence globally and obvious CRE difference with that of SL clouds. In the mean, global total cloud fraction was about 77.4%, while the SL and ML cloud fractions were 51.6% and 25.8%, respectively. The global mean SL and ML cloud amounts were 67.7% and 32.3%, respectively. Many previous studies showed that cloud fraction is a critical factor in cloud–radiation feedback [42,43]. To avoid the effect of cloud fraction on CRE, only clear and SL or ML overcast CERES footprints were used to investigate the CRE differences between ML and SL clouds.

Analysis of the CRE differences indicates that there are very obvious CRE differences between ML and SL clouds. Generally speaking, the zonal mean SW CRE differences between the ML and SL clouds at the TOA and surface

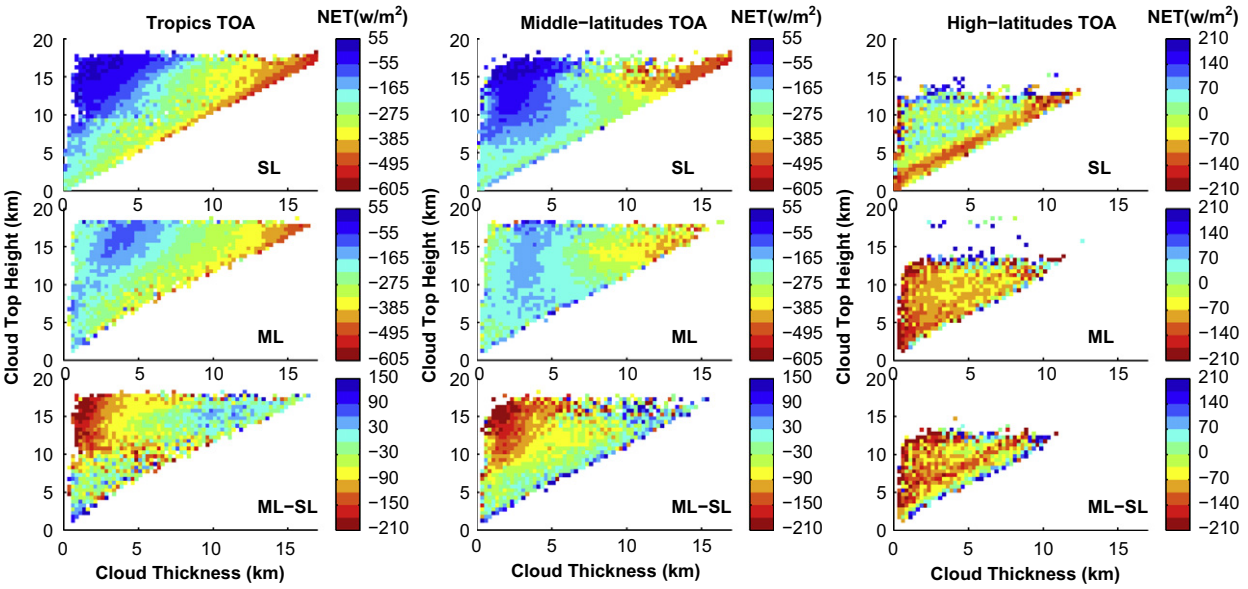

Fig. 12. Same as Fig. 11, except for 3 different latitudinal zones.

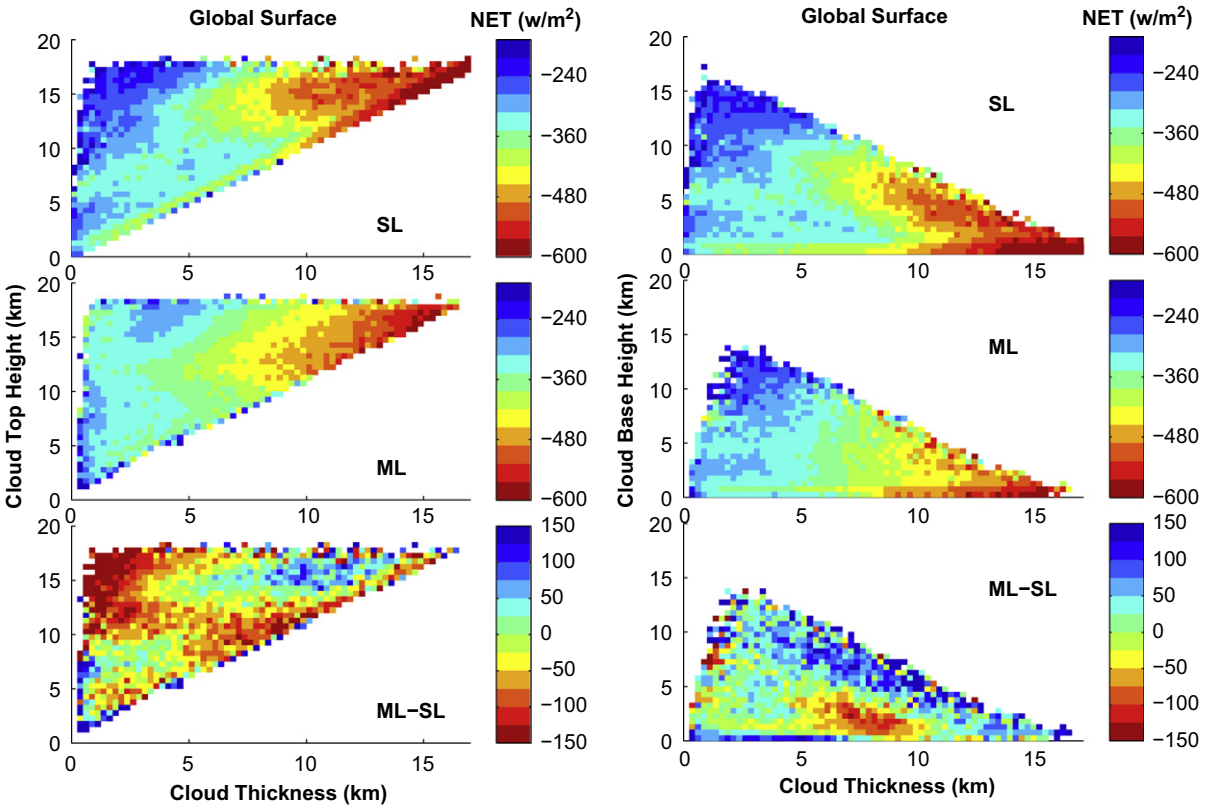

Fig. 13. Left panel is the same as Fig. 11, except for surface Net CRE. Right panel is same as left panel but as a function of cloud thickness and cloud base height.

were positive at most latitudes. It was clearly shown that thicker and higher clouds are dominant (left panel of Fig. 6 and upper panel of Fig. 9), and that thicker and higher clouds are prevalent over tropical oceans (left panel of Fig. 5). Their SW CRE difference maximum is at 120 W m^{-2} in the tropics and a minimum of -30 W m^{-2} at higher latitudes. This indicates that the ML clouds usually reflect less sunlight to the TOA and transmit more to the surface and within the atmosphere than the SL clouds as a whole. Therefore, the radiative fluxes at the surface and within the atmosphere may be underestimated when ML clouds are present due to the fact that radiative fluxes at the surface and within the atmosphere are generally retrieved by simply assuming that all clouds are single-layered (SL). The difference in zonal mean LW CRE between ML and SL clouds at the TOA was relatively small, ranging from -30 to 30 W m^{-2}. This showed that ML clouds only increase the amount of thermal radiation at the TOA relative to that of SL clouds in the tropics and decrease it elsewhere. In other words, the ML clouds tend to cool the atmosphere in the tropics and warm it elsewhere compared to the SL clouds. However, many studies on the radiation effect of ML clouds have mainly depended on various numerical models [11], some confirming that the radiation is sensitive to the cloud overlap assumption used [48,49]. Further, cloud horizontal inhomogeneity contributes to model uncertainty [10]. The results of the CRE difference showed that the zonal mean CRE difference between ML and SL clouds obtained by satellite observations is very obvious and smaller than the system difference of models using different cloud overlap assumptions. By not relying on a cloud overlap assumption and horizontal inhomogeneity, this approach will provide the observational basis for evaluating GCM model results and cloud overlap assumptions.

As the factors that influence the CRE are numerous and complicated, we performed a preliminary analysis at different latitude zones, only accounting for variables such as cloud top height (CTH), cloud layer thickness (CLT), and cloud base height (CBH). In summary, the same distribution trends are evident in the tropics and middle-latitudes, that is, the SW cloud cooling effect (negative SW CREs) increases with increasing CLT for both SL and ML clouds. When the clouds are high but relatively thin (cirrus and cirrostratus), the cloud cooling effect of the ML clouds is larger than that of SL clouds. When the clouds are high and thick (such as deep convective clouds), the SW cloud cooling effects for the SL and ML clouds are both large (the absolute values of SW CRE range from 300 to 600 W m^{-2}) but comparable since the differences of SW CRE between ML and SL clouds are relative small (range from -60 to 60 W m^{-2}). The SW CRE difference between ML and SL clouds is larger when the clouds are thinner and higher. The LW cloud warming effects

(positive LW CREs) increase with CTH and CLT for both SL and ML clouds. However, it is worth noting that the SW CRE is strongly positive at the mid- or high-latitudes in Figs. 7 and 8, but the zonal means are nearly all negative (Fig. 6). The results are mainly caused by solar zenith angles greater than 78°.

CRE is strongly dependent on cloud properties (e.g., cloud optical depth, phase, liquid water path, particle radius, cloud cover, type), and surface parameters (e.g., surface albedo, surface temperature) [50]. For example, by using a one-dimensional radiative convective model, Stephens and Webster [51] demonstrated that high thin clouds at low and mid-latitude in all seasons, and all cloud types at high latitudes in winter tend to warm the surface relative to a clear sky; all other clouds tend to cool the surface. Their models also showed that, for a given cloud type, a critical surface albedo may exist at which the cloud turns from cooling to warming the surface when the surface albedo increases. However, accurate retrieval of ML cloud properties remains a big challenge. Combining passive and active remote sensing observation may be an effective approach.

It is worth noting that, although the TOA radiation budget can be determined fairly accurately from satellite observations, the radiative fluxes at the surface and within the atmosphere are generally retrieved by simply assuming that all clouds are single-layered. Furthermore, retrievals of the cloud properties, such as cloud height, optical depth, phase and particle size [17,33,34], used in the flux estimates can be compromised because they are typically based on the SL cloud assumption. Thus, the SL CRE results at the surface are more reliable than the ML results, and the TOA results are more reliable than the surface results for both SL and ML clouds in our study. Due to the sparse distribution of ground-based radar and lidar sites, the accurate retrieval of surface radiative flux needs better parameterizations to account for cloud overlap in models and better retrieval of various ML cloud and surface parameters from satellite observation. For example, Chou and Suarez [52] presented parameterizations for single-scattering cloud properties, for the treatment of cloud overlapping, and for the scaling of cloud optical thickness in a horizontally inhomogeneous cloud situation and to reduce model computational burden. However, proper quantification of cloud radiative effects at the surface is dependent on the accuracy of ML cloud microphysical property retrievals, which can be obtained by combining passive and active remotely sensed observations.

Acknowledgements

This research is supported by the National Science Foundation of China under grants 40725015 and 40633017, and by the NASA Science Mission through the CALIPSO Project and the Radiation Sciences Program through the CERES Project. The CERES SSF and CALIPSO data were obtained from the NASA Earth Observing System Data and Information System, Langley Research Center Atmospheric Sciences Data Center (ASDC).

References

[1] Hartmann DL, Short DA. On the use of Earth radiation budget statistics for studies of clouds and climate. J Atmos Sci 1980;37:1233–50.
[2] Hahn CJ, Warren SG, London J, Chervin RM, Jenne R. Atlas of simultaneous occurrence of different cloud types over the ocean. NCAR Tech Note TN-201+STR, 1982. p. 212.
[3] Hahn CJ, Warren SG, London J, Chervin RM, Jenne R Atlas of simultaneous occurrence of different cloud types over land. NCAR Tech Note TN-241+STR, 1984. p. 216.
[4] Poore K, Wang J, Rossow WB. Cloud layer thicknesses from a combination of surface and upper-air observations. J Climate 1995;8:550–68.
[5] Wang J, Rossow WB, Zhang Y. Cloud vertical structure and its variations from a 20-yr global rawinsonde dataset. J Climate 2000;13:3034–56.
[6] Webster PJ, Stephens GL. Tropical upper-tropospheric extended clouds: inferences from winter MONEX. J Atmos Sci 1980;37:1521–41.
[7] Webster PJ, Stephens GL. Cloud–radiation interaction and the climate problem. In: Houghton J, editor. The global climate. Cambridge University Press; 1984. p. 63–78.
[8] Randall DA, Harshvardhan, Dazlich DA, Corsetti TG. Interactions among radiation, convection, and large-scale dynamics in a general circulation model. J Atmos Sci 1989;46:1943–70.
[9] Wang J, Rossow WB. Effects of cloud vertical structure on atmospheric circulation in the GISS GCM. J Climate 1998;11:3010–29.
[10] Wu XQ, Liang XZ. Radiative effects of cloud horizontal inhomogeneity and vertical overlap identified from a monthlong cloud-resolving model simulation. J Atmos Sci 2005;62:4105–12.
[11] Chen T, Zhang YC. Sensitivity of atmospheric radiative heating rate profiles to variations of cloud layer overlap. J Climate 2000;13:2941–59.
[12] Warren SG, Hahn CJ, London J. Simultaneous occurrence of different cloud types. J Climate Appl Meteor 1985;24:658–67.
[13] Tian L, Curry JA. Cloud overlap statistics. J Geophys Res 1989;94:9925–35.
[14] Liang XZ, Wang WC. Cloud overlap effects on GCM climate simulations. J Geophys Res 1997;102(D):11039–47.
[15] Barker HW, Stephens GL, Fu Q. The sensitivity of domain-averaged solar fluxes to assumptions about cloud geometry. Quart J R Meteorol Soc 1999;125:2127–52.
[16] Morcrette JJ, Christian J. The response of the ECMWF model to changes in the cloud overlap assumption. Mon Weather Rev 2000;128:1707–32.
[17] Stephens GL, Wood NB, Gabriel PM. An assessment of the parameterization of subgrid-scale cloud effects on radiative transfer. Part I: Vertical overlap. J Atmos Sci 2004;61:715–32.
[18] Baum BA, et al. Multilevel cloud retrieval using multispectral HIRS and AVHRR data: nighttime oceanic analysis. J Geophys Res 1994;99(D3):5499–514.
[19] Baum BA, Uttal T, Poellot M, Ackerman TP, Alavarez JM, et al. Satellite remote sensing of multiple cloud layers. J Atmos Sci 1995;52(23):4210–30.
[20] Lin B, Minnis P, Wielicki BA, Doelling DR, Palikonda R, Young DF, et al. Estimation of water cloud properties from satellite microwave and optical measurements in oceanic environments. II: Results. J Geophys Res 1998;103:3887–905.
[21] Chang FL, Li ZQA. Near-global climatology of single-layer and overlapped clouds and their optical properties retrieved from *Terra*/MODIS data using a new algorithm. J Climate 2005;18:4752–71.
[22] Huang JP, Minnis P, Lin B. Advanced retrievals of multilayered cloud properties using multispectral measurements. J Geophys Res 2005;110:D15S18, doi:10.1029/2004JD005101.
[23] Huang JP, Minnis P, Lin B. Determination of ice water path in ice-over-water cloud systems using combined MODIS and AMSR-E measurements. Geophys Res Lett 2006;33:L21801, doi:10.1029/2006GL027038.
[24] Minnis P, et al. Ice cloud properties in ice-over-water cloud systems using TRMM VIRS and TMI data. J Geophys Res 2007;112:D06206, doi:10.1029/2006JD007626.
[25] Winker DM, Hunt WH, McGill MJ. Initial performance assessment of CALIOP. Geophys Res Lett 2007;34:L19803, doi:10.1029/2007GL030135.
[26] Stephens GL, et al. CloudSat mission: performance and early science after the first year of operation. J Geophys Res 2008;113:D00A18, doi:10.1029/2008JD009982.

[27] Barnes WL, Pagano TS, Salomonson VV. Prelaunch characteristics of the moderate resolution imaging spectroradiometer (MODIS) on EOS–AM1. IEEE Trans Geosci Remote Sens 1998;36:1088–100.
[28] Wielicki BA, Barkstorm BR, Harrison EF, Lee III RB, Smith GL, Cooper JE. Clouds and the Earth's radiant energy system (CERES): an Earth observing system experiment. Bull Am Meteorol Soc 1996;77:853–68.
[29] L'Ecuyer TS, Wood NB, Haladay T, Stephens GL, et al. Impact of clouds on atmospheric heating based on the R04 Cloudsat fluxes and heating rates data set. J Geophys Res 2008;113:D00A15.
[30] Loeb NG, Kato S, Loukachine K, Smith NM. Angular distribution models for top-of-atmosphere radiative flux estimation from the clouds and the Earth's radiant energy system instrument on the *Terra* satellite. Part I: Methodology. J Atmos Oceanic Technol 2005;22:338–51.
[31] Loeb NG, Kato S, Loukachine K, Smith NM. Angular distribution models for top-of-atmosphere radiative flux estimation from the clouds and the Earth's radiant energy system instrument on the Terra satellite. Part II: Validation. J Atmos Ocean Technol 2007;24: 564–84.
[32] Stackhouse PW, et al. Fast longwave and shortwave flux (FLASH-Flux) products from CERES and MODIS measurements. In: Proceedings of the 12th conference on atmospheric radiation. American Meteorological Society, Madison, Wisconsin, 2006 (available at 〈http://ams.confex.com/ams/pdfpapers/113479.pdf〉).
[33] Minnis P, et al. Cloud detection in non-polar regions for CERES using TRMM VIRS and Terra and Aqua MODIS data. IEEE Trans Geosci Remote Sens 2008;46:3857–84.
[34] Minnis P, et al. CERES Edition-2 CLOUD PROPERTY RETRIEVALS using TRMM VIRS and Terra and Aqua MODIS data. Part I: algorithms. IEEE Trans Geosci Remote Sens, submitted for publication (available at 〈http://www-pm.larc.nasa.gov/ceres/pub/journals/CERES.Retrieval.TGARS.09.1o.pdf〉).
[35] Darnell WL, Staylor WF, Gupta SK, Ritchey NA, Wilber AC. Seasonal variation of surface radiation budget derived from ISCCP-C1 data. J Geophys Res 1992;97:15741–60.
[36] Gupta SK, Kratz DP, Stackhouse Jr PW, Wilber AC The langley parameterized shortwave algorithm (LPSA) for surface radiation budget studies (version 1.0). NASA/TP-2001-211272, 2001. 31 p.
[37] Gupta SK, Darnell WL, Wilber AC. A parameterization for longwave surface radiation from satellite data: recent improvements. J Appl Meteor 1992;31:1361–7.
[38] Mace GG, et al. A description of hydrometeor layer occurrence statistics derived from the first year of merged Cloudsat and CALIPSO data. J Geophys Res 2009;114:D00A26, doi:10.1029/2007JD009755.
[39] Mace GG, et al. CloudSat Project: Level 2 radar-lidar GEOPROF product version 1.0 process description and interface control document, 2007. 9 p.
[40] Ramanathan V. The role of Earth radiation budget studies in climate and general circulation research. J Atmos Sci 1987;37:447–54.
[41] Cess RD, Potter GL. Exploratory studies of cloud RF with a general circulation model. Tellus 1987;39A:460–73.
[42] Fung IY, Harrison DE, Lacis AA. On the variability of the net longwave radiation at the ocean surface. Rev Geophys Space Phys 1984;22:177–93.
[43] Rossow WB, Lacis AA. Global, seasonal cloud variations from satellite radiance measurements. Part II: Cloud properties and radiative effects. J Climate 1990;3:1204–53.
[44] Hagihara Y, Okamoto H, Yoshida R. Development of a combined CloudSat/CALIPSO cloud mask to show global cloud distribution. J Geophys Res 2010:D00A26, doi:10.1029/2009JD012344.
[45] Winker D, Getzewitch B, Vaughan M Evaluation and applications of cloud climatologies from CALIOP. In: 24th International laser radar conference (ILRC). Boulder, CO, USA, 2008.
[46] Wylie DP, Jackson DL. Trends in global cloud cover in two decades of HIRS observations. J Climate 2005;18:3021–31.
[47] Mace GG, Benson S. The vertical structure of cloud occurrence and RF at the SGP ARM site as revealed by 8 years of continuous data. J Climate 2008;21:2591–610.
[48] Kuhn WR. The effects of cloud height, thickness, and overlap on tropospheric terrestrial radiation. J Geophys Res 1978;83:1337–46.
[49] Stubenrauch CJ, Del Genio AD, Rossow WB. Implementation of subgrid cloud vertical structure inside a GCM and its effect on the radiation budget. J Climate 1997;10:273–87.
[50] Shupe MD, Intrieri JM. Cloud radiative forcing of the Arctic surface: the influence of cloud properties, surface albedo, and solar zenith angle. J Climate 2004;17:616–28.
[51] Stephens GL, Webster PJ. Clouds and climate: sensitivity of simple systems. J Atmos Sci 1981;38:235–47.
[52] Chou MD, Suarez MJ. Parameterizations for cloud overlapping and shortwave single-scattering properties for use in general circulation and cloud ensemble models. J Climate 1998;11:202–14.